Remote Sensing of Environment 282 (2022) 113256

Contents lists available at ScienceDirect

Remote Sensing of Environment

journal homepage: www.elsevier.com/locate/rse

The potential of spaceborne GNSS reflectometry for detecting ocean surface currents

Mostafa Hoseini *, Hossein Nahavandchi

Department of Civil and Environmental Engineering, Norwegian University of Science and Technology (NTNU), Trondheim 7491, Norway

ARTICLE INFO

Edited by Menghua Wang

Keywords:
GNSS reflectometry
Small satellites remote sensing
Ocean surface currents
Wind–current interactions
Ocean surface roughness
Bistatic radar cross section

ABSTRACT

The detectability of ocean surface currents in global navigation satellite system reflectometry (GNSS-R) observations is analyzed. We use a large dataset of spaceborne GNSS-R measurements from NASA cyclone GNSS (CYGNSS) mission. The data is collocated with ocean wind and near-surface current measurements. Our analysis reveals clear responses of the GNSS-R σ_0 to the presence of currents. The response depends on the wind conditions and is more prominent for wind speeds below 6 m/s. A current velocity of 0.5 m/s under an opposing wind can, on average, suppress the GNSS-R σ_0 by 0.8 decibels for low incidence angles. The interaction of the same current with a codirectional wind can enhance σ_0 by almost the same amount. This enhancement is most visible at high incidence angles. We develop a model that improves the prediction of the GNSS-R σ_0 in the presence of surface currents. The detected signatures of wind–current interactions highlight the potential of GNSS-R sensors onboard small satellites for observing ocean surface currents.

1. Introduction

The earth-reflected signals of global navigation satellite systems (GNSS) can be collected and processed in a technique known as GNSS reflectometry (GNSS-R). Several remote sensing applications currently use this relatively new technique. The potential of this technique in combination with small satellite technology has led to the successful launch and operation of the eight microsatellites of the Cyclone GNSS (CYGNSS) mission, which have been producing continuous data streams since March 2017. Currently, various geophysical parameters on the Earth's surface can be monitored through spaceborne GNSS-R observations, with an average revisit time of approximately 7 h (Ruf et al., 2018). This study introduces the potential of spaceborne GNSS-R for a novel application, i.e. the detection of ocean surface currents at scales smaller than those covered by radar altimetry.

The movement of water from one location to another is referred to as oceanic currents, which are mainly driven by tides, wind, and thermohaline circulation generated by density differences (NOAA). Oceanic currents are known to alter ocean wave characteristics and influence sea states. It has been shown that the wave height variations at scales of 10–100 km mainly stem from the variations in the currents at the same scales (Ardhuin et al., 2017). The idea of measuring currents by utilizing the interaction between currents and gravity waves was formulated and studied a few decades ago by Huang et al. 1972. In that study, current-modified frequency and wavenumber spectra were introduced based on the laws of energy conservation and kinematic wave conservation. The proposed spectra account for the current–wave energy interchange that occurs in a particular frequency band when a wave field enters a region with a current. Fig. 1(a–c) shows the modified wavenumbers for wind speeds of 5, 10, and 15 m/s under different current conditions. This figure shows significant changes in the spectral characteristics under the influence of a current. The changes for the case of a 5 m/s wind speed include relatively significant changes in the magnitudes and locations of the energy peaks. These variations in the wavenumber spectrum can be translated into current-induced changes in the ocean surface roughness as represented by the mean squared slope (MSS). Within our analysis, we could not confirm that the changes predicted by the Huang et al. 1972 model can adequately describe the impact of surface currents on GNSS-R measurements. Therefore, to predict the effects of currents on GNSS-R observations, we develop and utilize an empirical model based on our numerical investigations and an MSS model proposed by Katzberg et al. 2006, hereafter referred to as the KZ model.

The KZ model relates the GNSS-R MSS measurements to the wind speeds at 10-meter height (U_{10}) through the following equations:

$$\begin{aligned} \xi_{||}(U_{10}) &= 0.45\,(0.000 + 0.00316\,f(U_{10})) \\ \xi_{\perp}(U_{10}) &= 0.45\,(0.003 + 0.00192\,f(U_{10})) \\ \xi_T\,(U_{10}) &= \xi_{||}(U_{10}) + \xi_{\perp}(U_{10}) \end{aligned} \tag{1}$$

* Corresponding author.
E-mail address: mostafa.hoseini@ntnu.no (M. Hoseini).

https://doi.org/10.1016/j.rse.2022.113256
Received 7 March 2022; Received in revised form 19 August 2022; Accepted 1 September 2022
Available online 23 September 2022

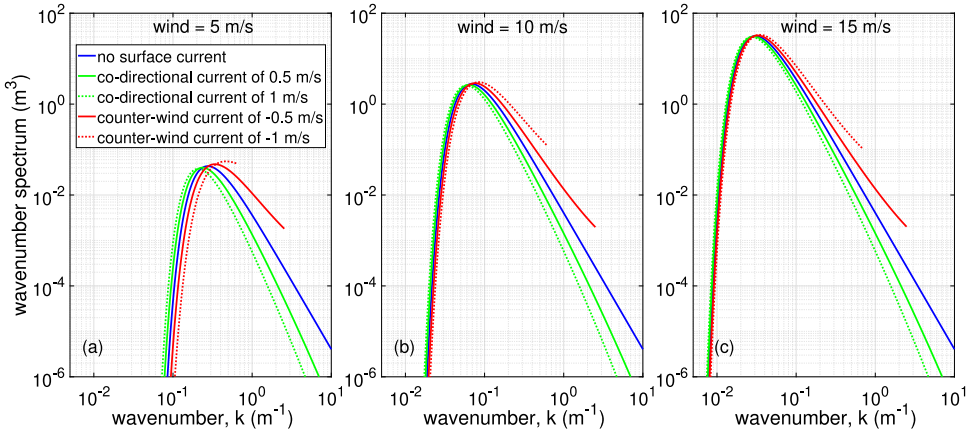

Fig. 1. Wavenumber spectra for wind speeds of (a) 5 m/s, (b) 10 m/s and (c) 15 m/s under different current conditions. The spectra were produced based on the wind–current wavenumber spectrum model of Huang et al. 1972. The spectra associated with counterwind currents have cutoff wavenumbers since the dispersion relationship is invalid beyond these cutoff thresholds.

where $\xi_{||}$ and $\xi_{\perp}$ are the MSS values parallel to and perpendicular to the wind, respectively. ξ_T is the total MSS in omnidirectional context according to the definition suggested by Elfouhaily et al. 1997. The piecewise function $f(U_{10})$ is defined as follows:

$$f(U_{10}) = U_{10} \qquad 0.00 < U_{10} \leq 3.49$$
$$f(U_{10}) = 6\ \ln(U_{10}) - 4.0 \qquad 3.49 < U_{10} \leq 46.00 \tag{2}$$

MSS estimates can be related to GNSS-R normalized bistatic cross section (NBRCS, σ_0) measurements through the following equation (Ruf et al., 2016):

$$\sigma_0(\theta, \varepsilon, U_{10}) = \frac{|R(\theta, \varepsilon)|^2}{\xi_T(U_{10})} \tag{3}$$

where R is the Fresnel reflection coefficient for GNSS-R cross-polarization reflection (Cardellach et al., 2012), which is a function of the incidence angle (θ) and the permittivity of seawater (ε). The GNSS-R observations of ocean surface roughness can also be affected by several factors other than local winds, including surface currents, surfactants, and swells not generated by the local wind (Ruf et al., 2016). Consequently, the following question arises: "Can GNSS-R measurements of ocean surface roughness provide sufficient sensitivity to detect surface currents?" The influence of currents on spaceborne GNSS-R observations based on the model of Huang et al. 1972 has been simulated by Ghavidel and Camps 2016 and Li et al. 2020 for estimating electromagnetic bias and predicting delay-Doppler maps (DDMs) in the presence of currents, respectively. Moreover, a study on the signatures of mesoscale ocean eddies in GNSS-R observations (Hoseini et al., 2020) suggests that the interaction of the eddy surface current with the overpassing wind field can be one of the main reasons for the observed NBRCS anomalies over the eddies. However, the detectability of ocean current signatures in real GNSS-R observations has not received sufficient attention and requires numerical investigation.

2. Data description

Our numerical investigation is based on GNSS-R measurements from the eight CYGNSS microsatellites. We use the NBRCS measurements from the level 1 data products (version 3.0) covering three years from January 2019 to December 2021. It should be noted that an earlier version of the data (version 2.1) covering a more extended period of about five years is also available. However, the newer version of the data used in this study provides higher quality measurements owing to an improved calibration process (e.g., Wang et al. 2021) and resolving some of the issues found in the earlier version (e.g., Said et al. 2018). The spatial coverage of the dataset includes latitudes between approximately 38°S and 38°N. The data is publicly available to users through the physical oceanography distributed active archive center (PODAAC) website of the national aeronautics and space administration (NASA) (CYGNSS, 2018).

The NBRCS values are computed using the so-called clean-replica approach. In this approach, the received reflections from the Earth's surface are cross-correlated with the receiver-generated pseudorandom noise (PRN) codes of global positioning system (GPS) satellites to estimate the power of the reflected signals. Then, the estimated power values are calibrated for several influencing factors and normalized to yield the NBRCS (σ_0) measurements. More details on the CYGNSS data products can be found in Ruf et al. 2016. The CYGNSS σ_0 samples are accompanied by quality flags. We filter out all the samples that are marked with the flag *poor_overall_quality*.

This analysis utilizes two ancillary datasets. The first dataset includes wind measurements from the European center for medium-range weather forecasts (ECMWF) reanalysis 5 (ERA-5), with a temporal resolution of one hour and a spatial resolution of 0.25 degrees (Hersbach et al., 2018). The ERA-5 global wind estimates are based on the assimilation of ground-based and satellite-based observations. The ocean surface current analysis real-time (OSCAR) dataset (ESR, 2018), with a temporal resolution of five days and a spatial resolution of 0.33 degrees, is the second ancillary dataset. Due to the lower temporal resolution of the OSCAR dataset, our analysis only considers the dates on which the surface current measurements are available. Based on this criterion, approximately 3.9×10^8 GNSS-R NBRCS measurements distributed on 219 days (73 days per year) are obtained from the CYGNSS dataset. The ERA-5 and OSCAR measurements are then used in a spatial–temporal linear interpolation process to estimate the wind speed and surface current at the GNSS-R reflection points.

The surface current data obtained from the OSCAR dataset and ERA-5 wind measurements are provided in two components, i.e., eastward and northward components. These components can be used to form wind and current vectors at GNSS-R specular points. The current vector can be decomposed into two orthogonal components based on the wind vector direction. Our analysis utilizes the along-wind component of the current vector shown in Fig. 2.

3. Signatures of ocean currents in spaceborne GNSS-R measurements

The overall influence of ocean surface currents on the GNSS-R σ_0 measurements can be seen in the histograms in Fig. 3(a–f). The distribution of σ_0 in the absence of ocean surface currents is shown in Fig. 3(a) and repeated in panel (d). The NBRCS values represented by red dashed line are based on the KZ model shown in (4) and can reasonably well describe the distribution pattern. However, the accuracy

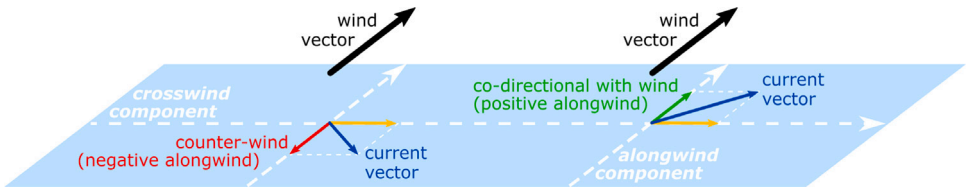

Fig. 2. Decomposition of the surface current vector based on the wind vector direction.

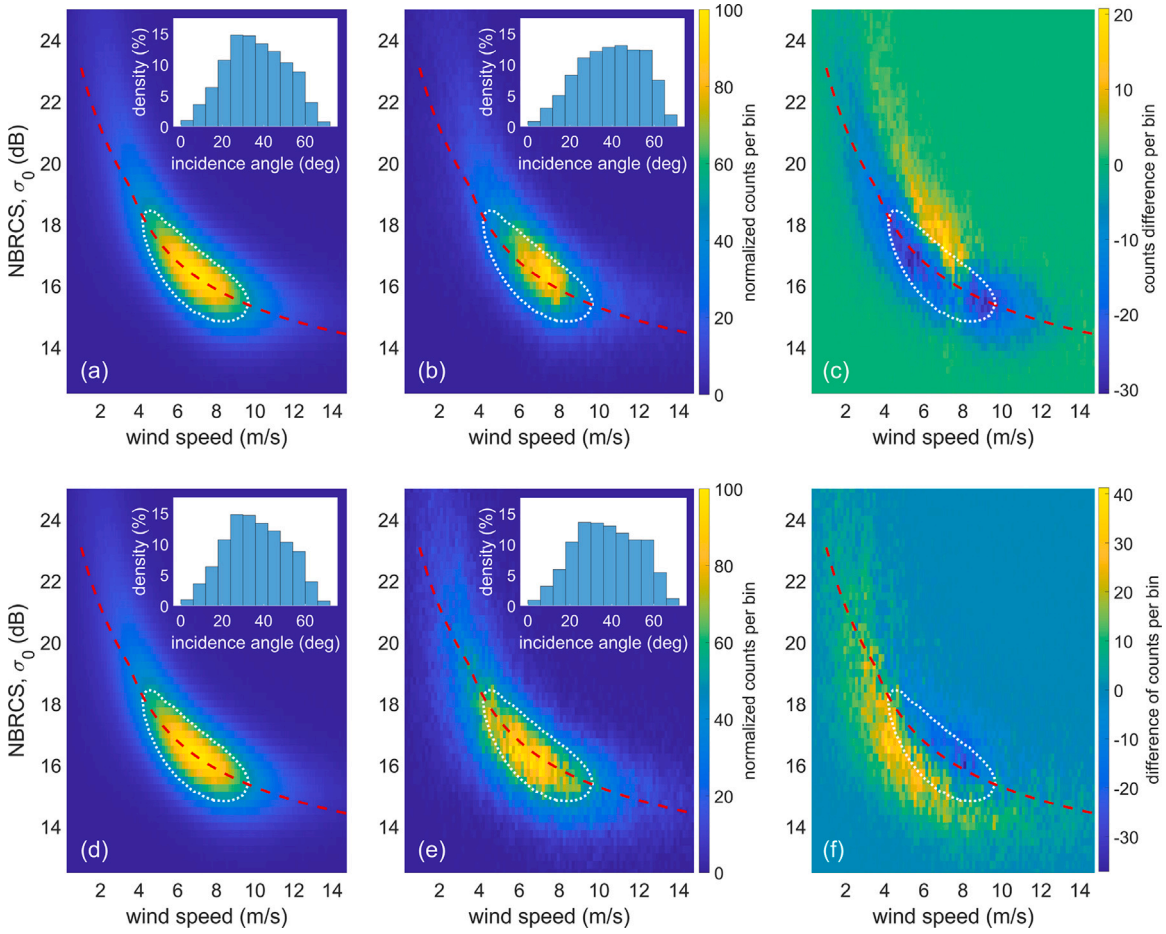

Fig. 3. The distributions of the CYGNSS normalized bistatic radar cross section (NBRCS) measurements under (a)/(d) no surface current, (b) codirectional currents and winds, and (e) counterwind currents are shown. Panels (c) and (f) show the difference between the histograms of codirectional currents with winds and counterwind currents with respect to no current condition, respectively. The incidence angle histograms associated with the measurements are overlaid on the plots. The white dots overlaid on the histograms depict a single level contour line retrieved from the current-free histogram in (a)/(d) and repeated in other panels for comparison purpose.

of the model predictions degrades in the presence of surface currents. Fig. 3(b) shows a concentration of σ_0 values above the predicted values when the currents and winds are codirectional. Panel (e) in this figure additionally reveals a change in the σ_0 distribution under counterwind currents, in which case the wind-only KZ model overestimates the σ_0 values. The histograms (c) and (f), which are calculated by subtracting histogram (a/d) from the panels (b) and (c), respectively, highlight the changes in the σ_0 concentration patterns during the wind–current interactions.

The σ_0 measurements and corresponding MSS values grouped based on various criteria are shown in the left and right columns of Fig. 4, respectively. This figure highlights the clear responses of the NBRCS measurements to ocean surface currents. In each panel of this figure, the data are divided into three groups based on the current conditions. The blue lines correspond to measurements collected under almost no surface current, i.e., current velocities lower than 0.05 m/s. The green and red colors correspond to measurements recorded under positive and negative along-wind currents, respectively, with a velocity of approximately 0.5 m/s (±0.1 m/s). The plots in the figure are split into three rows for the cases of low, moderate, and high incidence angles.

Overall, Fig. 4 suggests that the suppressed σ_0 values and boosted surface roughness observed under counterwind currents can be seen in any of the three ranges of incidence angle. However, this effect is less prominent for the grazing-angle measurements shown in Fig. 4(e) and (f). An opposing current exerts its most significant impact on GNSS-R observations at low to moderate incidence angles for wind speeds below 6 m/s. At incidence angles of 0 to 10 degrees, the average σ_0 reduction due to a counterwind current with a velocity of ≈ 0.5 m/s can reach approximately 0.8 decibels (dB) at 2 m/s wind speed, gradually declining to about 0.2 dB at 7 m/s wind. These values correspond to the relative increase of approximately 23% and 5% in the MSS values, respectively. The effect of a codirectional current with the wind on the GNSS-R σ_0 measurements is also evident in all the incidence angle ranges, although it is more pronounced for grazing-angle reflections

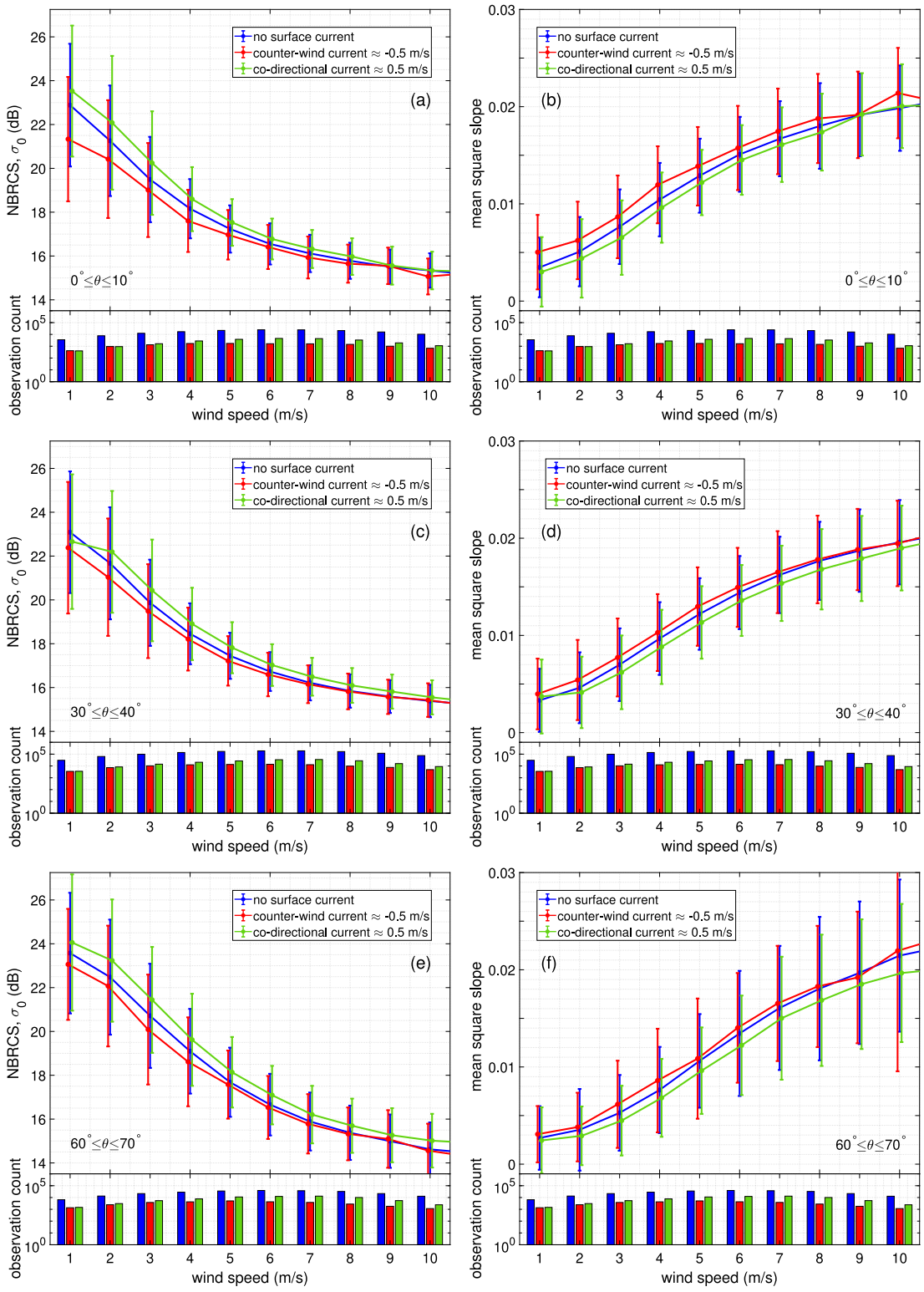

Fig. 4. A numerical assessment of current–wind interactions based on spaceborne GNSS-R measurements. The plots in the left column represent NBRCS measurements recorded under various current conditions, i.e., no surface current, a negative along-wind current (counterwind current) of 0.5 m/s, and a positive along-wind current (current codirectional with the wind) of 0.5 m/s. The plots in the right column depict the MSS estimates associated with the NBRCS measurements shown on the left. The graphs presented in different rows correspond to different ranges of incidence angles (θ), as noted on each plot. The histogram below each panel shows the numbers of observations used to calculate the graphs.

shown in the third row. The smoothed ocean surface in the presence of a +0.5 m/s along-wind current can elevate the average NBRCS value by approximately ≈ 0.8 dB for 2 m/s wind speed at high incidence angles of 60 to 70 degrees. This effect corresponds to a decline of approximately 18% in the MSS value. At these incidence angles, the effect of the codirectional current remains visible for even higher wind speeds. At 10 m/s wind, the average NBRCS increase is about 0.4 dB corresponding to %8 decrease in the corresponding MSS value.

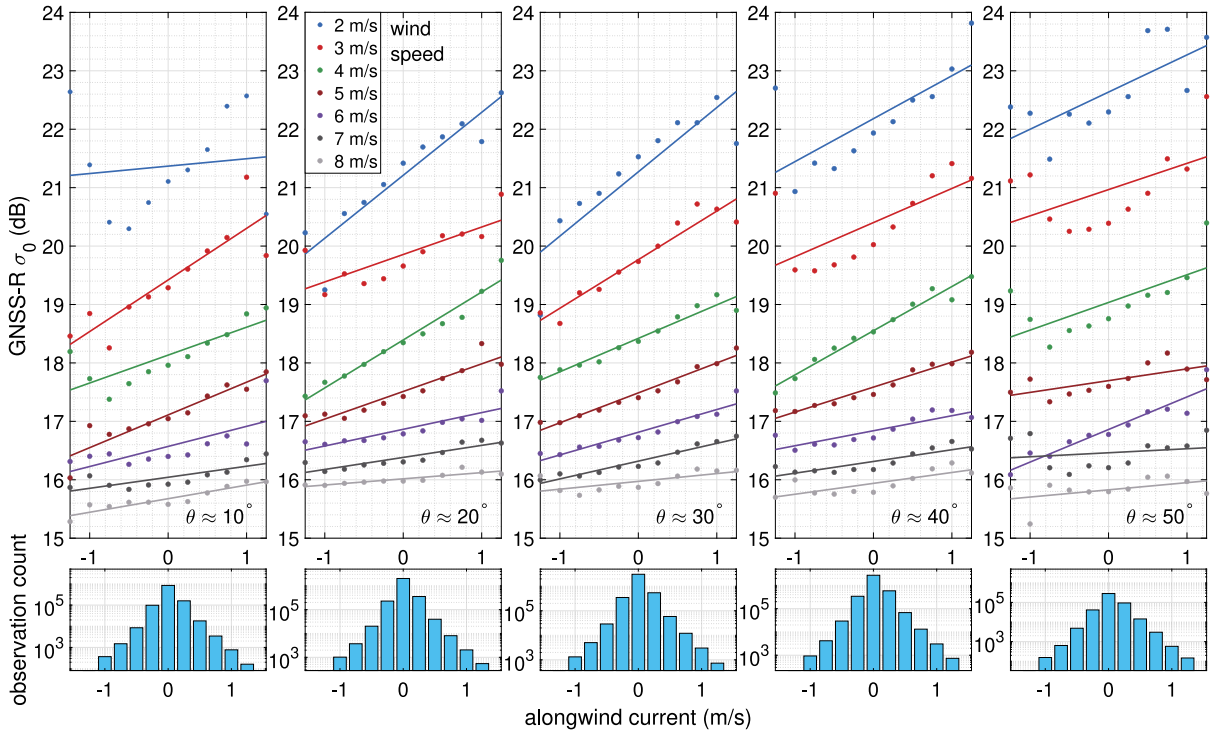

Fig. 5. Variation of GNSS-R σ_0 as a function of different parameters, including along-wind current, incidence angle, and wind speed.

The GNSS-R σ_0 change rates for a range of −1.25 to +1.25 m/s along-wind current at different incidence angles under 2 to 8 m/s wind speeds are depicted in Fig. 5. As can be seen in the figure, the rate of change in all of the incidence angles are gradually decreased with the increase of wind speed.

4. A wind–current model for GNSS-R measurements

The MSS models that are functions of solely wind speed can, in particular, miss a significant contribution to the MSS value from the larger wavenumbers close to the right tail of the spectrum in Fig. 1(a–c). This contribution corresponds to short waves and is known to be mainly influenced by two processes: the wind-generated surface stress and the short-wave – current interaction (Plant, 1982; Phillips, 1984). We develop a model to predict spaceborne GNSS-R σ_0 measurements in the presence of surface currents. This model uses the KZ empirical model for the initial estimation of the MSS. A least-squares refit of the KZ total MSS model based on the CYGNSS dataset under no-current condition is as follows:

$$\xi_T(U_{10}) = 0.45\ (0.00312 + 0.00417\ f(U_{10})) \tag{4}$$

with the function $f(U_{10})$ defined in (2). Using (3) and (4), the GNSS-R σ_0 in dB scale can be calculated by:

$$\sigma_{0\,dB} = 10\ \log_{10}\left(\frac{|R|^2}{\xi_T}\right) = |R|^2_{dB} - \xi_{T\,dB} \tag{5}$$

where $|R|^2_{dB}$ and $\xi_{T\,dB}$ are the squared Fresnel reflection coefficient and the total MSS value in dB scale, respectively. The wind-only model (4) together with (5) can be used to predict the σ_0 values based on different wind speeds. The σ_0 values predicted by this model exhibit a bias pattern shown in Fig. 6.

The bias patterns shown in Fig. 6 are calculated under different surface current conditions. In all the three panels of this figure, the NBRCS measurements associated with high incidence angles under wind speeds below 6 m/s show significant enhancements. The enhancements can be associated with the presence of the coherent reflection component in the received signals. The enhancements can be further amplified where there are codirectional currents and winds (Fig. 6(b)). In contrast, counterwind currents can suppress such enhancements and shift the pattern towards negative values indicated by the blue color (Fig. 6(c)). Therefore, the model is required to account for the combined effects of wind, surface current, and incidence angle. For developing such a model, we first reformulate the KZ total MSS model in terms of the following rational function:

$$\xi_T(U_{10})_{dB} = -\frac{P(U_{10})}{Q(U_{10})} = -\frac{n_2\ U_{10}^2 + n_1\ U_{10} + n_0}{U_{10}^2 + d_1\ U_{10} + d_0}\ , \quad U_{10} \le 46\ \text{m/s} \tag{6}$$

$$\begin{cases} n_2 = 13.481 \\ n_1 = 104.988 \\ n_0 = 135.721 \end{cases}\ , \qquad \begin{matrix} d_1 = 4.347 \\ d_0 = 4.834 \end{matrix}$$

$$\sigma_{0\,dB} = |R|^2_{dB} + \frac{P(U_{10})}{Q(U_{10})} \tag{7}$$

The reformulated KZ model offers a unified equation, in contrast to the piece-wise function described by (1) and (2). The quadratic single-variable function $P(U_{10})$ in (6) can be extended to a multi-variable form to include the effects of surface current and incidence angles as well:

$$\xi_T(U_{10}, U_c, \theta)_{dB} = -\frac{P(U_{10}, U_c, \theta)}{Q(U_{10})} \tag{8}$$

$$\sigma_{0\,dB} = |R|^2_{dB} + \frac{P(U_{10}, U_c, \theta)}{Q(U_{10})} \tag{9}$$

with U_c being the along-wind current velocity. The extended quadratic function reads:

$$\begin{aligned} P(U_{10}, U_c, \theta) &= n_9\ U_{10}^2 + n_8\ U_c^2 + n_7\ \theta^2 + \\ &= n_6\ U_{10} + n_5\ U_c + n_4\ \theta + \\ &= n_3\ U_{10}\ U_c + n_2\ U_{10}\ \theta + n_1\ U_c\ \theta + n_0 \end{aligned} \tag{10}$$

with $\{n_0, \ldots, n_9\}$ and $\{d_0, d_1\}$ being the unknown coefficients of our wind–current model. The incidence angle (θ) in (10) is in radian. We divide the collocated dataset into two parts for model training and

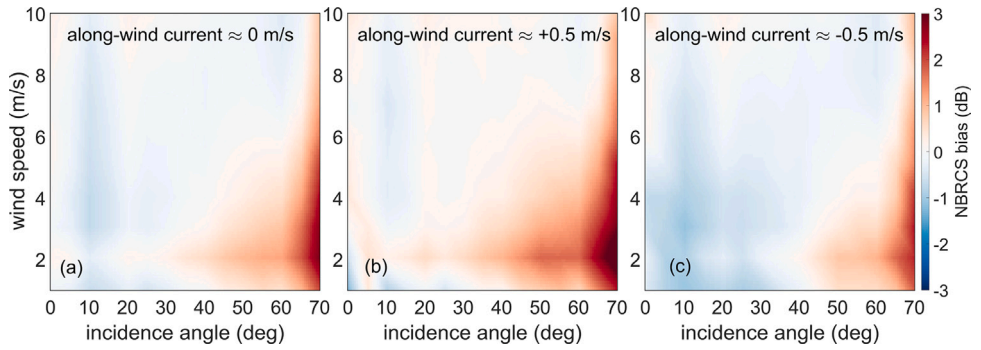

Fig. 6. The bias between the observed and predicted NBRCS measurements under (a) no current condition, (b) currents of 0.5 m/s codirectional with wind field, and (c) currents of 0.5 m/s opposing to the wind. The predicted NBRCS is calculated using the KZ model shown in (4).

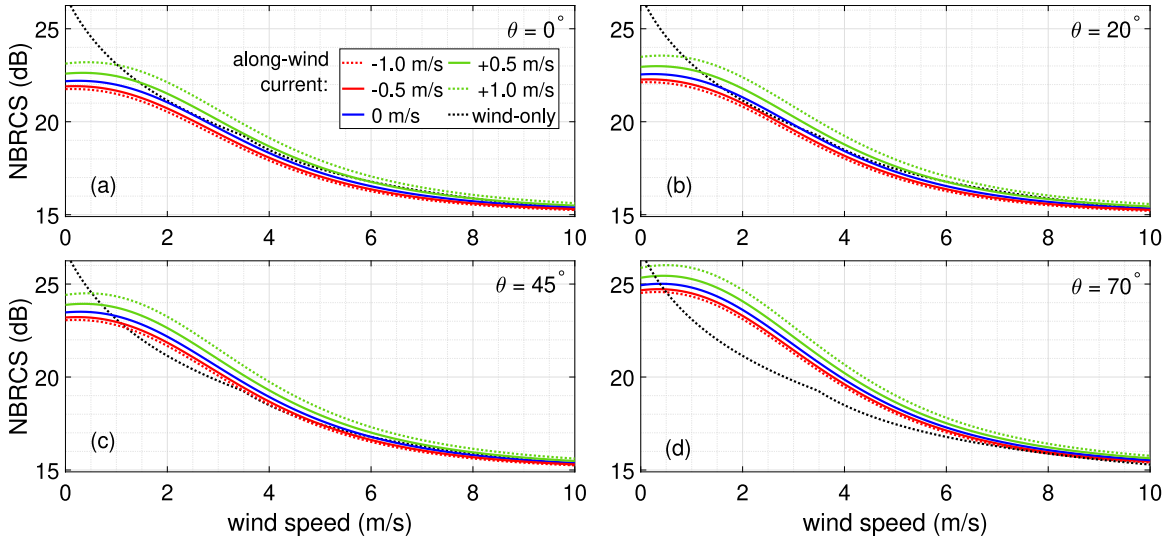

Fig. 7. Predicted σ_0 values using the developed wind–current model at different incidence angles (θ). The solid and dotted green lines represent currents with speeds of 0.5 and 1 m/s, respectively, which are codirectional with the wind. The solid and dotted red lines represent counterwind currents with speeds of 0.5 and 1 m/s, respectively. The blue line corresponds to the zero-current condition, and the dotted black line corresponds to the wind-only KZ model.

validation purposes. The first part consists of two years worth of data, including the GNSS-R measurements in 2019 and 2020, which are used for the calculation of the coefficients in (10). The remaining one-year data in 2021 is used for the performance assessment. The 12 coefficients $\{n_0, \ldots, n_9, d_0, d_1\}$ are estimated through iterative minimization of the root mean square error (RMSE) of the predicted σ_0 with respect to the observed values. The initial estimates of the coefficients used in the calculation are provided from the reformulated KZ model in (6). The calculated coefficients of the model are listed as follows:

$$\begin{cases} n_9 = 17.425 & n_6 = -63.641 & n_3 = 0.381 & n_0 = 447.705 \\ n_8 = 4.886 \quad , & n_5 = 12.838 \quad , & n_2 = -3.139 \quad , & d_1 = -2.797 \\ n_7 = 26.040 & n_4 = 10.456 & n_1 = -0.170 & d_0 = 18.718 \end{cases} \tag{11}$$

Fig. 7(a-d) shows the predicted σ_0 values using the developed model at four incidence angles under different wind speeds and current velocities. The black dotted line in each panel corresponds to σ_0 calculated using the wind-only KZ model in (4). The predictions of the modified model in Fig. 7 show that the impact of surface currents is better visible at low wind speeds, while the accumulated impact of the bias and current effects is significant at high incidence angles.

The performance of the KZ wind-only model described by (4) and the developed model is represented in Fig. 8(a) and (b), respectively. In these maps, the color of each pixel represents the regional correlation between the actual GNSS-R σ_0 observed by CYGNSS in 2021 and the model-predicted counterparts. A performance comparison of the two models is presented in Fig. 8(c), where the improvement of the correlation coefficient is shown. The figure highlights that the wind–current model proposed in this study has an improved prediction capability by including the role of ocean surface currents. This improvement is noticeable over the regions associated with strong ocean currents; it can reach to 6% for equatorial currents, while for the California current and the Gulf Stream, lower level of improvement is observed. However, there are also some regions where slight performance degradation of about -1% can be seen, e.g., in the Indian Ocean or the middle of the Pacific Ocean.

Our investigation shows that despite the improved performance of the developed model compared to the wind-only KZ model, the effect of surface currents could be underestimated in our model. The reason for this issue can be associated with the utilized wind measurements from the ERA-5 dataset. Scatterometric wind speed retrievals as one of the observation sources assimilated into ERA-5 (Hersbach et al., 2020) is based on the wind-generated surface stress, which is a measure of the relative wind speed with respect to the ocean surface velocity (Seo et al., 2016). The surface stress can be estimated by (Seo et al., 2016):

$$\tau = \rho_a \, C_D \, (U_{10} - U_c) \, |U_{10} - U_c| \tag{12}$$

with τ being the surface stress, ρ_a the density of air, and C_D the drag coefficient. According to (12), a current codirectional with wind can reduce the magnitude of the surface stress, and a current in the opposing direction with respect to wind can increase the magnitude of surface stress. Therefore, scatterometric wind measurements with

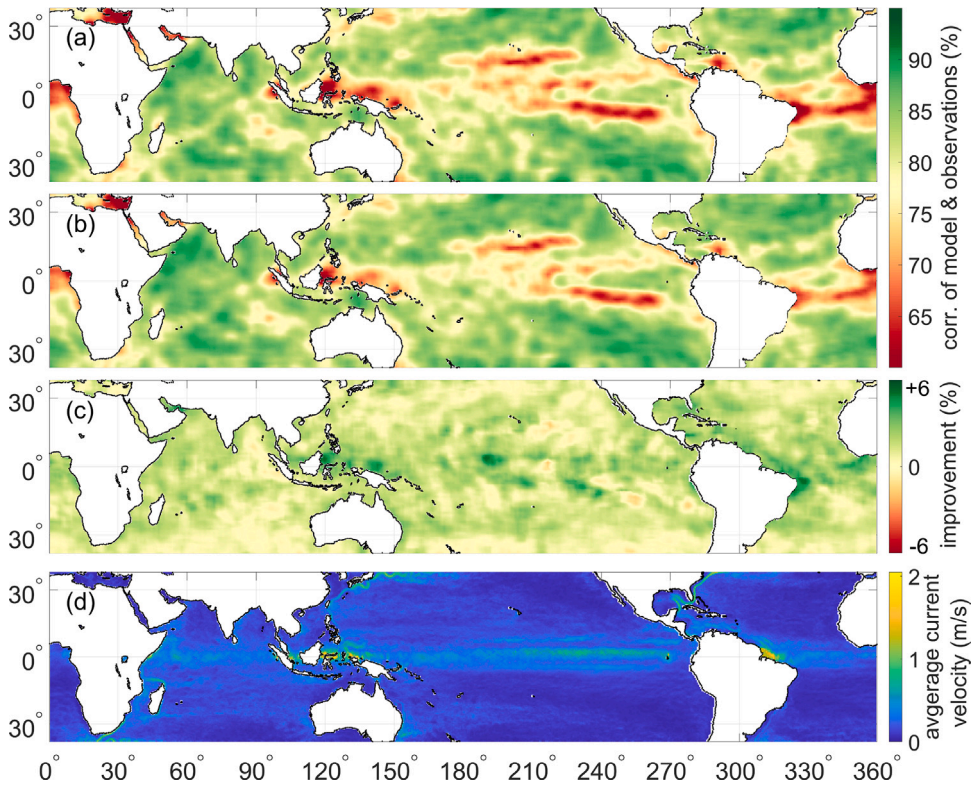

Fig. 8. Correlation maps between the observed GNSS-R NBRCS measurements from the CYGNSS mission and the predicted values from (a) the KZ model as a function of wind, and (b) the model developed in this study as a function of wind and current. Panel (c) shows the improvement in the correlation coefficient between the observed and modeled NBRCS values when the surface current is included in the model. The maps are created using one year of the CYGNSS level-1 data in 2021. Panel (d) is a global average map of current velocity based on the OSCAR dataset.

the signatures of currents could have affected our analysis. In order to improve the performance of the developed model, we repeat the modeling process using a subset of the training dataset. The subset includes samples at which along-wind currents and MSS anomaly, defined as follows, have the same sign.

$$\Delta MSS = MSS_{U_c=0} - MSS_{obs} \tag{13}$$

where ΔMSS is the MSS anomaly, $MSS_{U_c=0}$ is the predicted MSS value when the along-wind current is zero, i.e., using the model in (4), and MSS_{obs} is the observed MSS value from GNSS-R σ_0 observations. The observations in the training subset will fulfill the condition:

$$U_c \,.\, \Delta MSS > 0 \tag{14}$$

with U_c being the along-wind component of the surface current. The selected observations in the training subset use the following rationale. Let us consider a region where MSS is mainly governed by the local wind and its interaction with a surface current. Over such a region, an observed larger MSS value compared to wind-only conditions, i.e., $\Delta MSS < 0$, is associated with the counterwind component of the current ($U_c < 0$). In contrast, a $\Delta MSS > 0$ will be due to the positive along-wind component of the current ($U_c > 0$). These effects can be confirmed by the theoretical model shown in Fig. 1, and the observed signatures in Fig. 4 and Fig. 5.

For the performance assessment purpose, we apply the same selection criterion to the measurements in 2021 to form the corresponding evaluation subset. The new estimations of the model coefficients in (9) and (10) based on the described training subset are:

$$\begin{cases} n_9 = 16.20 & n_6 = -18.33 & n_3 = 4.95 & n_0 = 336.40 \\ n_8 = -13.44 \;, & n_5 = 56.74 \;, & n_2 = 0.44 \;, & d_1 = -0.94 \\ n_7 = 19.52 & n_4 = -11.14 & n_1 = 12.63 & d_0 = 13.33 \end{cases} \quad \forall\ |U_c| < 1.5 \tag{15}$$

Using these coefficients we can reproduce the graphs shown in Fig. 7(a-d). Fig. 9(a-d) shows the predicted σ_0 values using the new estimation of the coefficients. In contrast to Fig. 7, all the panels of Fig. 9 show more pronounced current effects. The corresponding correlation maps shown in Fig. 10 confirm that the predicted GNSS-R σ_0 values based on the coefficients in (15) provide significantly better performance. The improvement map shown in Fig. 10(c) highlights improvements exceeding 20% and exhibits a clear correspondence with the average current velocities depicted in Fig. 10(d).

The performance of the developed model compared to the KZ model can also be evaluated by the RMSE values shown in Fig. 11 and Table 1. The results confirm that the developed wind–current model provides an improved overall performance. The overall RMSE values of the wind-only and wind–current models for the evaluation subset over 2021 are 1.63 and 1.38 dB, respectively, which highlights 15.3% improvement. It should be highlighted that for strong counterwind currents with velocities larger than 1 m/s, the predicted σ_0 values using the developed model performs worse. The GNSS-R observations under these strong counterwind currents account for a minimal data share of about 0.05% (Table 1). This can be one of the factors contributing to the lower level of performance. Another contributing factor could be possible insufficient model flexibility to capture anomalies associated with the strong negative along-wind currents. However, Table 1 confirms that the developed model can effectively predict GNSS-R σ_0 over 99.95% of the observations.

Fig. 12 illustrates the effects of currents on the GNSS-R σ_0 through three exemplary cases for negative and positive along-wind currents. The first example, shown in Fig. 12(a), is related to a CYGNSS track passing over the western Indian Ocean close to the southern coasts of Mozambique. The colored specular points in Fig. 12(a_1) show the variation in σ_0 values. The specular points are overlaid on light blue points with different sizes as indicators of the surface current strength. A profile representation of the track is shown in Fig. 12(a_2). The time

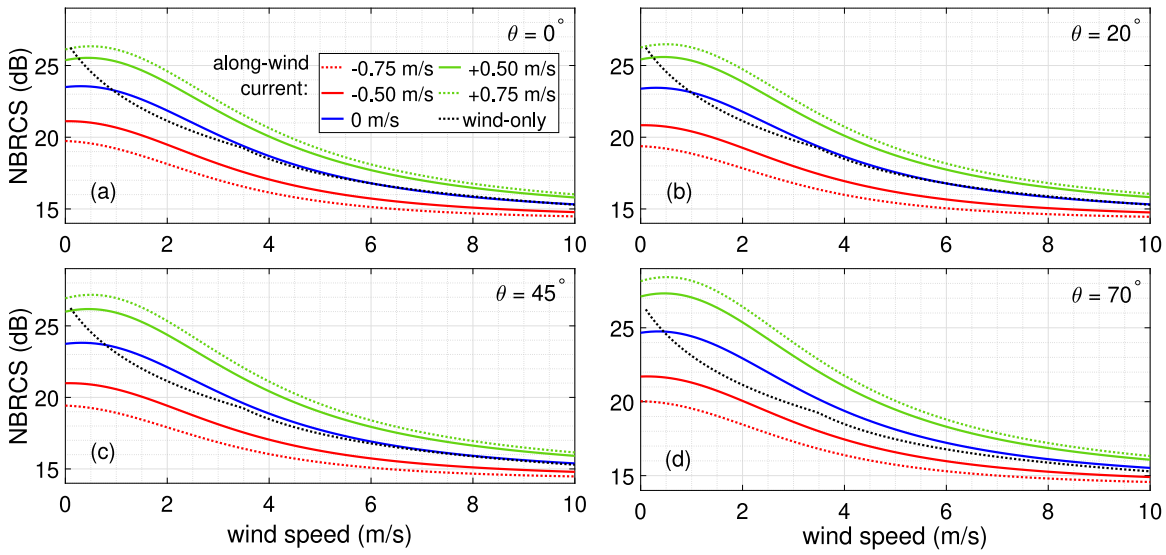

Fig. 9. Predicted σ_0 values using the developed wind–current model at different incidence angles (θ) based on the coefficients in (15). The solid and dotted green lines represent currents with speeds of 0.5 and 0.75 m/s, respectively, which are codirectional with the wind. The solid and dotted red lines represent counterwind currents with speeds of 0.5 and 0.75 m/s, respectively. The blue line corresponds to the zero-current condition, and the dotted black line corresponds to the wind-only KZ model. (For interpretation of the references to color in this figure legend, the reader is referred to the web version of this article.)

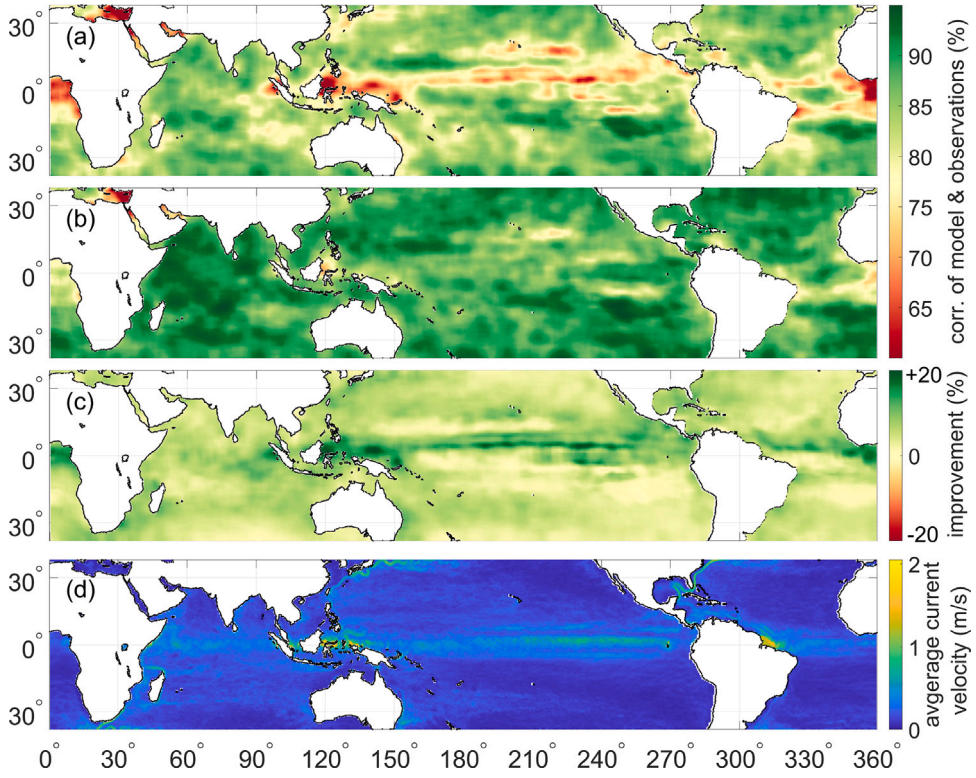

Fig. 10. Correlation maps between the observed GNSS-R NBRCS measurements from the CYGNSS mission and the predicted values from (a) the KZ model as a function of wind and (b) the model developed in this study as a function of wind and current. Panel (c) shows the improvement in the correlation coefficient between the observed and modeled NBRCS values when the surface current is included in the model. Panel (d) is a global average map of current velocity based on the OSCAR dataset.

series of NBRCS values are aligned with the wind speed and the along-wind component of the surface current in Fig. 12(a_3). The track passes over a region with wind speeds varying between about 5 to 8 m/s. The highest wind speed occurs at the middle of the track where a codirectional current with a velocity of 1 m/s exists. Interestingly, the fluctuations of the GNSS-R σ_0 profile reflect both effects of wind and current very well. When the track passes over the region with the surface current, the NBRCS profile rises by about 1 dB. The wind-only model shown in the dotted gray line in Fig. 12(a_2) completely misses the increase of observed GNSS-R σ_0 (brown line) due to the presence of current. In comparison, the developed wind–current model represented by a solid dark gray line provides better predictions of the σ_0 values.

Fig. 12(b) is related to the second exemplary case in the middle of the Pacific Ocean. The specular points over the equatorial current of about 1.2 m/s experience prominently higher σ_0 values by about 5 dB compared to the rest of the track. The lower wind speeds in this region

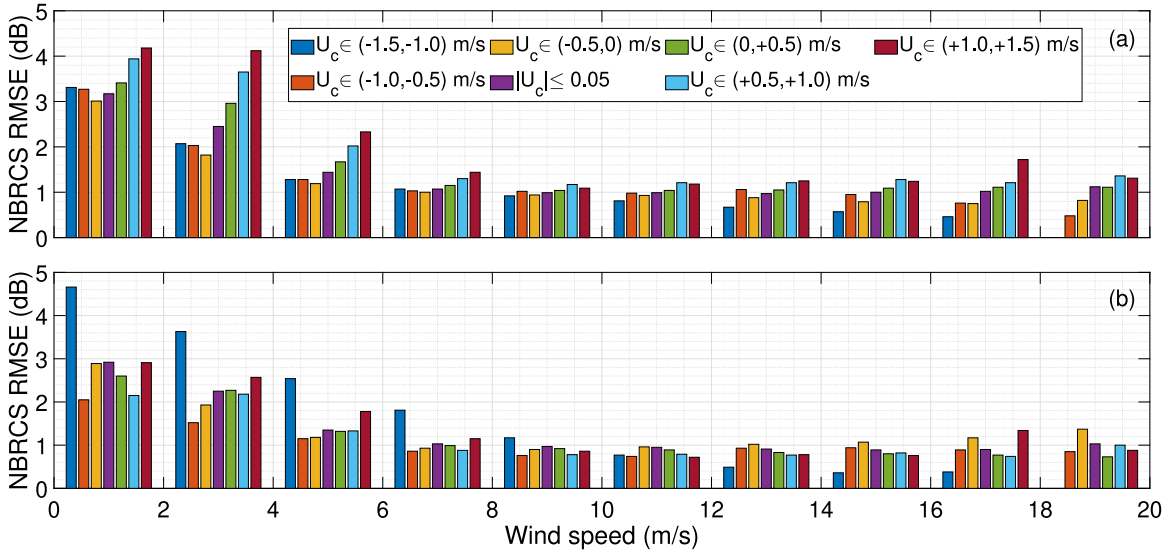

Fig. 11. Root mean square errors (RMSE) of the predicted GNSS-R σ_0 using (a) the KZ wind-only model based on (4) and (b) the developed wind–current model based on the coefficients shown in (15). The parameter U_c refers to the along-wind current velocity.

Table 1
A performance overview of the predicted GNSS-R σ_0 using the KZ wind-only model based on (4) (entries with white background) and the developed wind–current model (entries with gray background) based on the coefficients shown in (15). The table entries are the root mean square errors of the model-predicted values with respect to the observed σ_0 from the CYGNSS mission. The parameter U_c refers to the along-wind current velocity.

Wind (m/s)	Along-wind current velocity (m/s)						
	(−1.5,−1)	(−1,−0.5)	(−0.5,0)	$\lvert U_c \rvert \leq 0.05$	(0,+0.5)	(+0.5,+1.0)	(+1.0,+1.5)
0–2	3.31	3.27	3.01	3.17	3.41	3.94	4.18
	4.66	2.05	2.89	2.92	2.60	2.13	2.91
2–4	2.07	2.03	1.82	2.45	2.96	3.65	4.12
	3.63	1.52	1.93	2.25	2.27	2.18	2.57
4–6	1.28	1.28	1.19	1.44	1.67	2.02	2.33
	2.54	1.15	1.18	1.35	1.32	1.33	1.78
6–8	1.07	1.03	1.00	1.07	1.15	1.30	1.44
	1.81	0.86	0.93	1.03	0.99	0.88	1.15
8–10	0.92	1.02	0.94	0.99	1.04	1.17	1.09
	1.17	0.76	0.90	0.97	0.92	0.78	0.86
Data share	**0.05%**	**0.61%**	**40.95%**	|	**56.60%**	**1.64%**	**0.14%**

can partially justify the elevated NBRCS values. The dotted gray line (the wind-only model) in Fig. 12(b_2) describes the role of the lower wind. However, the predicted σ_0 profile shown by the dark gray line (the wind–current model) highlights that the inclusion of the current effect is required to describe this track's NBRCS variations.

The third exemplary case, presented in Fig. 12(c), depicts a track passing over the Kuroshio current close to the coast of Japan. A prominent enhancement of GNSS-R σ_0 by about 0.8 dB is seen in the beginning part as the track enters the strong current region with a positive along-wind component. As the dotted gray line in Fig. 12(c_2) shows, the KZ wind-only model follows the wind speed, which has almost the highest speed of the profile (≈13 m/s) at the beginning of the track. The wind effect alone fails to justify the elevated values of the NBRCS over the beginning part of the track. In contrast, a significant improvement by our developed model can be observed in this region (the solid gray line in Fig. 12(c_2)). The developed model shows another improvement in the middle part of the track when a counterwind current of about 0.5 m/s flows. Over this region, the GNSS-R NBRCS profile manifests enough sensitivity to detect the interaction of the wind and current and shows a reduction of about 0.5 dB.

5. Discussion and conclusions

The effects of ocean surface currents on spaceborne GNSS-R σ_0 measurements are numerically investigated. An empirical model is developed and evaluated based on a large number of observations from the CYGNSS mission during 2019–2021. In the analysis, the signatures of current-induced changes in the MSS, as an indicator of sea surface roughness, are detected.

We find that low wind speeds below 6 m/s can provide favorable conditions for observing the signatures of surface currents. GNSS-R NBRCS measurements at different incidence angles exhibit slightly different sensitivities to currents that are in the same and opposite directions with respect to the wind. Currents codirectional with the wind can significantly suppress the surface roughness, leading to an augmented σ_0. This effect is more pronounced at high incidence angles. In contrast, counterwind currents boost the MSS value, resulting in a reduced σ_0. The NBRCS difference between the two cases, i.e., positive and negative along-wind currents, can exceed 1.5 dB for a current velocity of approximately 0.5 m/s.

The model developed in this study, which accounts for the combined effects of wind and currents, shows improved performance in predicting the GNSS-R NBRCS, particularly over regions associated with stronger surface currents. The correlation of the predicted GNSS-R σ_0 by the

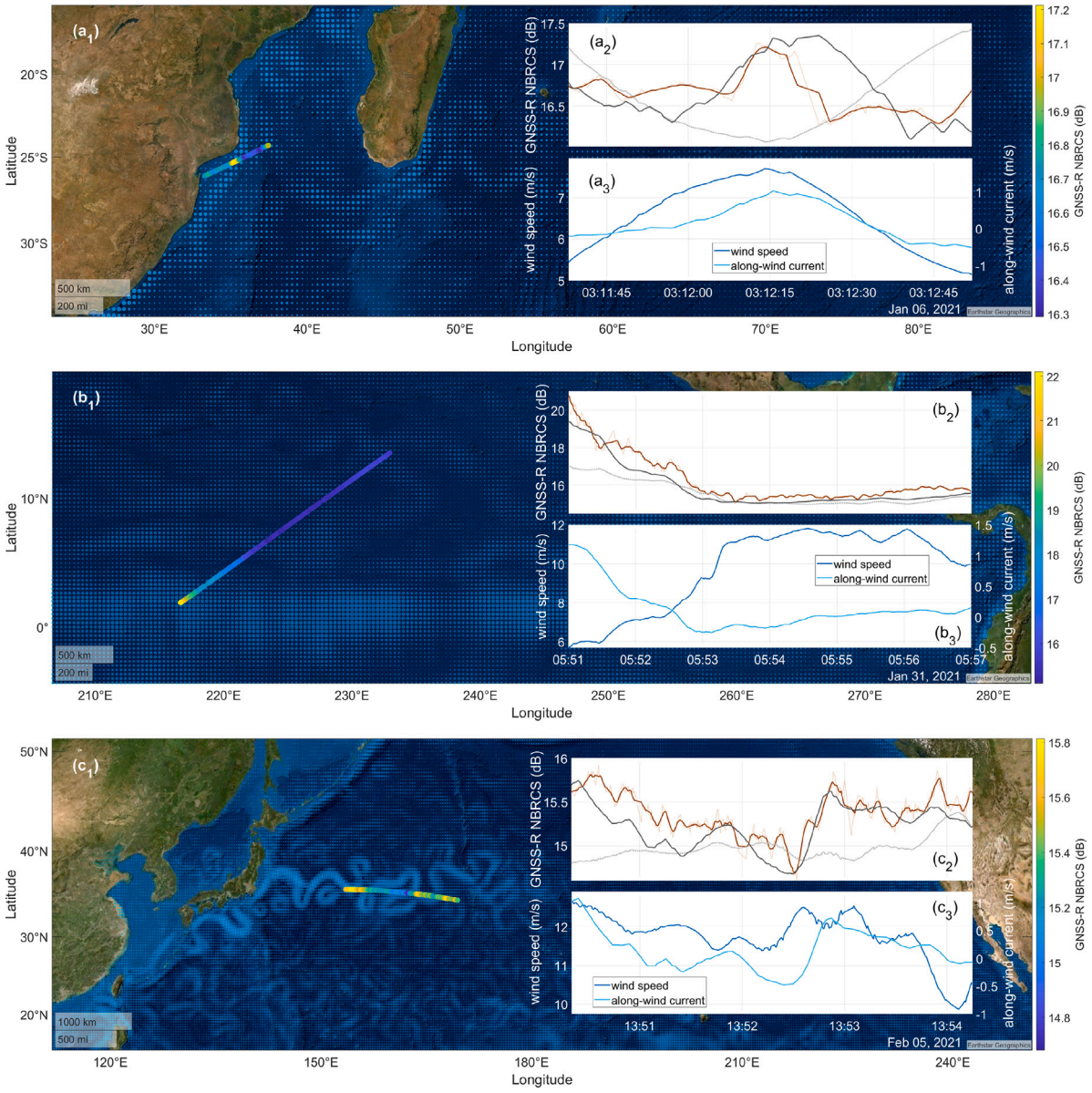

Fig. 12. Illustration of the impact of ocean surface currents on spaceborne GNSS-R measurements. The colored scatter plots in (a_1), (b_1) and (c_1), with the corresponding color bars on the right, show the evolution of the GNSS-R NBRCS when the tracks pass over different surface currents. The size of the light blue circles overlaid on the ocean reveals the strength of the surface currents. In (a_2), (b_2) and (c_2), the light and dark brown graphs are related to the original and smoothed NBRCS values, respectively, and the solid and dotted gray graphs correspond to the KZ wind-only model and the wind–current model introduced in this study, respectively. Panels (a_3), (b_3) and (c_3) present the collocated wind and ocean current information, with separate y-axes on the left and right, respectively.

developed model with the observed σ_0 is noticeably higher compared to the wind-only counterpart over the equatorial regions with high-velocity currents. Moreover, the overall RMSE of the wind–current model is about 15% lower compared to the wind-only model. The results of our analysis suggest that GNSS-R sensors onboard small satellites can provide sufficient sensitivity to detect the interaction of ocean surface currents with the overpassing wind fields.

It should be noted that besides the interaction of winds and currents, several other factors, including swells, surfactants, and precipitation, can alter the spaceborne GNSS-R σ_0 observations. The influence of these factors can affect the accuracy of GNSS-R wind speed measurements. For example, a surface current opposing the wind field can lead to a larger MSS value, which will be translated to an overestimated wind speed. This overestimation can also be observed when a non-locally generated swell enters the region and increases the surface roughness. On the other hand, the suppressing effect of surfactants on the ocean surface roughness can also result in an underestimation of the wind intensity. Further studies are encouraged to develop a combined model that simultaneously accounts for the described affecting factors.

CRediT authorship contribution statement

Mostafa Hoseini: Conceptualization, Methodology, Software, Data curation, Writing – original draft, Investigation, Visualization. **Hossein Nahavandchi:** Supervision, Writing – reviewing and editing, Funding acquisition.

Declaration of competing interest

Mostafa Hoseini reports a relationship with Helmholtz Centre Potsdam German Research Centre for Geosciences that includes: non-financial support and travel reimbursement.

Data availability

Data will be made available on request.

Acknowledgments

This study is supported by the Norwegian University of Science and Technology (NTNU). The authors would like to express their gratitude to the editor and three anonymous reviewers for reviewing the manuscript and making valuable suggestions and comments, which have helped us improve the quality of the manuscript. We also thank the CYGNSS and OSCAR teams for making the corresponding datasets publicly available through the PODAAC website at https://podaac.jpl.nasa.gov/CYGNSS and https://podaac.jpl.nasa.gov/dataset/OSCAR_L4_OC_third-deg, respectively. The ERA-5 dataset from ECMWF is also acknowledged for the wind dataset that is freely available at https://doi.org/10.24381/cds.adbb2d47. The model developed in this study is provided as a supplementary file for this paper.

Appendix A. Supplementary data

Supplementary material related to this article can be found online at https://doi.org/10.1016/j.rse.2022.113256.

References

Ardhuin, F., Gille, S.T., Menemenlis, D., Rocha, C.B., Rascle, N., Chapron, B., Gula, J., Molemaker, J., 2017. Small-scale open ocean currents have large effects on wind wave heights. J. Geophys. Res. Oceans 122 (6), 4500–4517. http://dx.doi.org/10.1002/2016JC012413.

Cardellach, E., Fabra, F., Rius, A., Pettinato, S., D'Addio, S., 2012. Characterization of dry-snow sub-structure using GNSS reflected signals. Remote Sens. Environ. 124, 122–134.

CYGNSS, 2018. CYGNSS level 1 science data record version 2.1. Ver. 2.1. PO.DAAC, CA, USA. Dataset accessed [2019-01-26] at http://dx.doi.org/10.5067/CYGNS-L1X21.

Elfouhaily, T., Chapron, B., Katsaros, K., Vandemark, D., 1997. A unified directional spectrum for long and short wind-driven waves. J. Geophys. Res. Oceans 102 (C7), 15781–15796.

ESR, 2018. OSCAR third deg. 2009. Ver. 1. PO.DAAC, CA, USA. Dataset accessed [2019-01-26] at http://dx.doi.org/10.5067/OSCAR-03D01.

Ghavidel, A., Camps, A., 2016. Impact of rain, swell, and surface currents on the electromagnetic bias in GNSS-reflectometry. IEEE J. Sel. Top. Appl. Earth Obs. Remote Sens. 9 (10), 4643–4649.

Hersbach, H., Bell, B., Berrisford, P., Biavati, G., Horányi, A., Muñoz Sabater, J., Nicolas, J., Peubey, C., Radu, R., Rozum, I., et al., 2018. ERA5 hourly data on single levels from 1979 to present. In: Copernicus Climate Change Service (C3S) Climate Data Store. Vol. 10. CDS, Dataset accessed [2019-01-26] at http://dx.doi.org/10.24381/cds.adbb2d47.

Hersbach, H., Bell, B., Berrisford, P., Hirahara, S., Horányi, A., Muñoz-Sabater, J., Nicolas, J., Peubey, C., Radu, R., Schepers, D., et al., 2020. The ERA5 global reanalysis. Q. J. R. Meteorol. Soc. 146 (730), 1999–2049.

Hoseini, M., Asgarimehr, M., Zavorotny, V., Nahavandchi, H., Ruf, C., Wickert, J., 2020. First evidence of mesoscale ocean eddies signature in GNSS reflectometry measurements. Remote Sens. 12 (3), 542.

Huang, N.E., Chen, D.T., Tung, C.-C., Smith, J.R., 1972. Interactions between steady won-uniform currents and gravity waves with applications for current measurements. J. Phys. Oceanogr. 2 (4), 420–431.

Katzberg, S.J., Torres, O., Ganoe, G., 2006. Calibration of reflected GPS for tropical storm wind speed retrievals. Geophys. Res. Lett. 33 (18).

Li, B., Yu, B., Yang, L., Yang, D., Han, H., 2020. Modeling and simulation of GNSS-R signals with ocean currents. In: China Satellite Navigation Conference. Springer, pp. 99–110.

NOAA, 2022. What is a current? National ocean service website. https://oceanservice.noaa.gov/facts/current.html, (Accessed 25 June 22).

Phillips, O., 1984. On the response of short ocean wave components at a fixed wavenumber to ocean current variations. J. Phys. Oceanogr. 14 (9), 1425–1433.

Plant, W.J., 1982. A relationship between wind stress and wave slope. J. Geophys. Res. Oceans 87 (C3), 1961–1967. http://dx.doi.org/10.1029/JC087iC03p01961.

Ruf, C., Chang, P., Clarizia, M.-P., Gleason, S., Jelenak, Z., Murray, J., Morris, M., Musko, S., Posselt, D., Provost, D., et al., 2016. CYGNSS Handbook. Vol. 154. Michigan Pub, Ann Arbor, MI.

Ruf, C.S., Chew, C., Lang, T., Morris, M.G., Nave, K., Ridley, A., Balasubramaniam, R., 2018. A new paradigm in earth environmental monitoring with the cygnss small satellite constellation. Sci. Rep. 8 (1), 1–13.

Said, F., Jelenak, Z., Chang, P.S., Soisuvarn, S., 2018. An assessment of CYGNSS normalized bistatic radar cross section calibration. IEEE J. Sel. Top. Appl. Earth Obs. Remote Sens. 12 (1), 50–65.

Seo, H., Miller, A.J., Norris, J.R., 2016. Eddy–wind interaction in the california current system: Dynamics and impacts. J. Phys. Oceanogr. 46 (2), 439–459.

Wang, T., Ruf, C.S., Gleason, S., O'Brien, A.J., McKague, D.S., Block, B.P., Russel, A., 2021. Dynamic calibration of GPS effective isotropic radiated power for GNSS-reflectometry earth remote sensing. IEEE Trans. Geosci. Remote Sens. 60, 1–12.